# Low-temperature catalytic combustion of trichloroethylene over cerium oxide and catalyst deactivation

Qiguang Dai, Xingyi Wang *, Guanzhong Lu *

*Laboratory for Advanced Materials, Research Institute of Industrial Catalysis, East China University of Science and Technology, Shanghai 200237, PR China*

## Abstract

Cerium oxide catalysts prepared by a thermal decomposition method using the salt nitrate as precursor were tested for the catalytic combustion of trichloroethlyene (TCE), as a model of chlorinated volatile organic compounds (CVOCs). $CeO_2$ catalysts calcined at different temperature were found to possess high catalytic activity for catalytic combustion of TCE, and $CeO_2$ calcined at 550 °C was the most active catalyst and the complete combustion temperature ($T_{90\%}$) of TCE was 205 °C. Effects of systematic variation of reaction conditions, including space velocity, inlet TCE concentration and water concentration on TCE catalytic combustion were investigated. Additionally, the stability and deactivation of $CeO_2$ catalysts were studied by various characterization methods (such as TG/DTA, EDS, XRD, Raman and XPS) and other assistant experiments.
© 2008 Elsevier B.V. All rights reserved.

*Keywords:* Catalytic combustion; Chlorinated VOCs; Cerium oxide; Catalyst deactivation

## 1. Introduction

Environmental contamination resulted from volatile organic compounds (VOCs) is a matter of considerable current concern, since these VOCs are considered as being dangerous for their effect on human health and the environment. Among VOCs, chlorinated volatile organic compounds (CVOCs), such as dichloromethane (DCM), chloroform ($CHCl_3$), carbon tetrachloride ($CCl_4$), 1,2-dichloroethane (DCE), trichloroethylene (TCE) and tetrachloroethylene (PCE), require special attentions on account of their toxicity, high stability and widespread application in industry. Nowadays, CVOCs are a wide range class of solvents commonly found in industrial waste streams and widely used in the chemical industry, including such processes as vinylchloride producing, dry cleaning, paint stripping and metal degreasing, due to their excellent solvency and virtual non-flammability. However, their improper disposal has led to groundwater and soil contamination, even destroyed the ozone layer. Therefore, their destruction or safe disposal is

an immediate national need. Besides thermal incineration, several catalytic technologies removing CVOCs, such as catalytic combustion or destruction, photocatalytic destruction, catalytic steam reforming and catalytic hydrodechlorination are used widely. Thermal incineration has been a conventional treatment method for any VOCs, but it requires the operating temperature ranging from 800 to 1000 °C and consumes lots of energy. In addition, the thermal incineration also can lead to the formation of incomplete combustion products such as highly toxic by-products. Recently, photocatalytic destruction [1,2] and catalytic hydrodechlorination [3–5] of CVOCs have received great interest, but their application in treatment of industrial waste gases may be limited due to the necessary of ultraviolet light or hydrogen sources. Because of high conversions possible at high space velocities, the catalytic steam reforming [6–8] promises to be an attractive approach for the destruction of chlorocarbons found in many industrial waste streams, but it requires usually higher temperature (700–900 °C) and the catalyst deactivation is also caused by parallel thermal pyrolysis reactions.

Catalytic combustion is an effective and the most popular technology to reduce the emissions of VOCs from waste gases, and is widely studied in the elimination of CVOCs. Catalytic combustion of CVOCs may be carried out at lower operating

* Corresponding authors. Tel.: +86 21 642533372; fax: +86 21 64253703.
  *E-mail addresses:* wangxy@ecust.edu.cn (X. Wang), gzhlu@ecust.edu.cn (G. Lu).

temperature (300–550 °C) and lower concentration of pollutants (<0.1%) than thermal incineration. Another major advantage of catalytic combustion is the potential selectivity towards the formation of harmless reaction products, such as $CO_2$, $H_2O$ and HCl. Most of the previous work related to catalysts for CVOCs catalytic combustion is focused on the development of two types of catalysts, namely those based on noble metals [9–12] and transition metal oxides [13–20]. Noble metal catalysts such as Pt, Pd, Rh and Ru are very active for the destruction of CVOCs, but the halide (HCl and $Cl_2$ produced from the decomposition of CVOCs) deactivation is still avoidless [12,21]. Traditionally, supported transition metal oxides have been proposed as potential substitutes for noble metal-based catalysts [14]. Generally, transition metal oxides are less active than noble metals, but they are more resistant to deactivation [15]. Among transition metal oxide catalysts, chromium-based catalysts have exhibited the highest activity for CVOCs abatement [16,17]. Nevertheless, the use of this type of catalysts tends to be restricted owing to the formation of extremely toxic residues such as chromium oxychloride at low temperature [18]. Additionally, as well known, both noble metal and transition metal oxide catalysts can also be active in the Deacon and oxychlorination reactions, which lead to the formation of molecular chlorine and undesired higher chlorinated compounds. More recently, solid acidic catalysts [22–29], including H-type zeolites such as H-Y, H-ZSM-5 and H-mordenite, alumina and alumina-based materials, have been proposed for CVOCs catalytic destruction. It is well accepted in the literature that the activity is associated with the Brønsted acidity present in this type of catalysts. There is, however, a large amount of coke deposition over acidic catalysts during CVOCs catalytic destruction, which results in the catalyst deactivation. In addition, a plenty of higher chlorinated compounds are produced due to the co-presence of Lewis acidic sites in these solid acidic catalysts. In conclusion, the catalysts employed in catalytic combustion of CVOCs often present some problems such as their deactivation, high cost, relative low activity or the formation of undesired higher chlorinated compounds. Therefore, the selection and development of more suitable catalysts for eliminating CVOCs are still necessary.

Recently, cerium oxide has attracted much attention in environmental catalysis, either as an effective promoter or as a supporting material based on its high oxygen-storage capacity (OSC) and facile $Ce^{4+}/Ce^{3+}$ redox cycle [30–32]. Supported $CeO_2$ and $CeO_2$-based mixed oxides are cheap, environmentally friendly and efficient catalysts for catalytic decomposition of nonchlorinated VOCs [33–36], such as methane, methanol and propane, for the wet oxidation process of organic compounds in the industrial waste waters, and for the removal of total organic carbon (TOC) from polluted water [37,38]. González-Velasco [39] investigated the complete oxidation of VOCs/CVOCs over ceria–zirconia mixed oxides. The combination of surface acidity and accessible lattice oxygen appeared to control the catalytic performance of CVOCs over ceria–zirconia catalyst. Additionally, Lin and Wang [40–42] conducted a catalytic wet air oxidation of phenolic waste water and the catalytic incineration of aromatic hydrocarbons using $CeO_2$, and found that $CeO_2$ possessed high catalytic activity. However, the suitability of $CeO_2$ as catalyst for CVOCs catalytic combustion has been considered to a less extent.

In the present work, the suitability of $CeO_2$ catalysts for catalytic combustion of trichloroethylene (TCE) was investigated. The effect of calcinated temperature, space velocity, inlet TCE concentrations and water vapor on catalytic activity were evaluated in detail and the selectivity for HCl or $Cl_2$ with or without water was analyzed. Additionally, the stability of $CeO_2$ catalyst was examined, and the probable cause of the catalyst deactivation was investigated by assistant experiments.

## 2. Experimental

### 2.1. Catalysts preparation

$CeO_2$ catalysts were prepared by the thermal decomposition method using $Ce(NO_3)_3 \cdot 6H_2O$ (SCRC, 99.0%) as precursor at 450, 550, 650 and 800 °C for 5 h in air.

In order to investigate the catalyst deactivation, the fresh $CeO_2$ samples were treated by following methods:

(1) $CeO_2$ calcinated at 550 °C was impregnated in 2 M HCl aqueous solution at room temperature for 2 h, then washed with deionized water, and dried at 100 °C. The resulting material is marked with $CeO_2$–HCl.
(2) $CeO_2$–HCl was calcined at 550 °C for 4 h in air atmosphere, the air flow rate through the reactor was set at 50 $cm^3$ $min^{-1}$ and the gas hourly space velocity (GHSV) was maintained at 15,000 $h^{-1}$. The calcined $CeO_2$–HCl is marked with $CeO_2$–HCl–Air.
(3) $CeO_2$–HCl was calcined at 550 °C for 4 h in humid air atmosphere (12% (v/v) of water), the flow rate through the reactor was set at 50 $cm^3$ $min^{-1}$ and the gas hourly space velocity (GHSV) was maintained at 15,000 $h^{-1}$. The calcined $CeO_2$–HCl is marked with $CeO_2$–HCl–$H_2O$.
(4) $CeO_2$ was impregnated in the saturated NaCl solution at room temperature for 2 h, then washed with deionized water, and dried at 100 °C. The resulting material is marked with $CeO_2$–NaCl.

The catalytic activities of the treated $CeO_2$ catalysts were investigated for catalytic combustion of trichloroethylene under dry condition.

### 2.2. Catalysts characterization

#### 2.2.1. Powder X-ray diffraction

The powder X-ray diffraction patterns (XRD) of the samples were recorded on a Rigaku D/Max-rC powder diffractometer using Cu Kα radiation (40 kV and 100 mA). The diffractograms were recorded in the $2\theta$ range of 10–80° with a $2\theta$ step size of 0.01° and a step time of 10 s.

#### 2.2.2. Nitrogen adsorption/desorption

The nitrogen adsorption and desorption isotherms were measured at 77 K on an ASAP 2400 system in static measurement mode. The samples were outgassed at 160 °C

for 4 h before the measurement. The specific surface area was calculated using the BET model.

### 2.2.3. Energy dispersive spectroscopy

The analyses of the elements were carried out with an energy dispersive spectrometer (EDS) detector (EDAX Falcon) attached to SEM (JSM-6360LV).

### 2.2.4. Thermogravimetric analysis

Coke formation was evaluated with thermogravimetric analysis (TGA) using a PerkinElmer Pyris Diamond TG/TGA Setaram instrument. The fresh and used $CeO_2$ samples were heated up to 800 °C from room temperature (heating rate of 10 °C min$^{-1}$) in air stream.

### 2.2.5. Raman spectroscopy

The Raman spectra were obtained on a Renishaw in Viat + Reflex spectrometer equipped with a CCD detector at ambient temperature and moisture-free conditions. The emission line at 514.5 nm from an $Ar^+$ ion laser (Spectra Physics) was focused, analyzing spot about 1 mm, on the sample under the microscope. The power of the incident beam on the sample was 3 mW. Time of acquisition was varied according to the intensity of the Raman scattering. The wave numbers obtained from spectra were accurate to within 2 cm$^{-1}$.

### 2.2.6. X-ray photoelectron spectroscopy

The XPS measurements were made on a VG ESCALAB MK II spectrometer by using Mg K$\alpha$ (1253.6 eV) radiation as the excitation source. Charging of samples was corrected by setting the binding energy of adventitious carbon (C1 s) at 284.6 eV. The powder samples were pressed into self-supporting disks, loaded into a sub-chamber, and evacuated for 4 h, prior to the measurements at 298 K.

### 2.2.7. Temperature programmed desorption

Temperature programmed desorption (TPD) of $CO_2$ was performed in a quartz micro-reactor. 100 mg of sample was firstly loaded in the reactor and heated in flowing $N_2$ at 550 °C for 2 h. $CO_2$ was then introduced to the reactor after it was cooled down to 100 °C. To remove the weakly adsorbed $CO_2$, sample was swept using flowing $N_2$ at 100 °C for 2 h. The TPD experiments were then carried out in flowing $N_2$ with a flow rate of 30 ml min$^{-1}$ from 100 to 550 °C at a linear heating rate of 10 °C min$^{-1}$. The desorption of $CO_2$ was detected by a mass spectrum ($m/z = 44$).

$O_2$-TPD experiments were carried out in the same quartz micro-reactor. 100 mg of sample was loaded in a micro-reactor and heated in $N_2$ at 550 °C for 1 h (except the $CeO_2$ catalyst calcined at 450 °C), then $O_2$ flow was continuously passed at 20 ml min$^{-1}$ through samples for 0.5 h so that catalyst samples were completely oxidized. Then the samples were swept using flowing $N_2$ at 550 °C for 1 h, then cooled to 50 °C in $N_2$ flow (30 ml min$^{-1}$). When temperature was increased at a heating rate of 10 °C min$^{-1}$ from 50 up to 800 °C, the desorption of $O_2$ was detected by an INFICON Transpecter 2 quadrupole mass spectrometer ($m/z = 32$).

### 2.2.8. Temperature programmed reduction

$H_2$-temperature programmed reduction ($H_2$-TPR) of $CeO_2$ samples (150 mg) placed at the bottom of the U-shaped quartz tube was investigated by heating $CeO_2$ samples (150 mg) in $H_2$ (5 vol.%)/Ar flow (30 ml min$^{-1}$) at a heating rate of 10 °C min$^{-1}$ from 20 to 750 °C. The hydrogen consumption was monitored by thermo-conductivity detector (TCD). Before the $H_2$-TPR analysis, the samples were heated for 60 min in Ar flow at 300 °C, and then treated in $O_2$ at room temperature for 30 min.

### 2.3. Catalytic activity measurement

Catalytic combustion reactions were carried out in a continuous flow micro-reactor constituted of a U-shaped quartz tube of 4 mm of inner diameter at atmospheric pressure. 270 mg catalyst was placed at the bottom of the U-shaped microreactor. The feed flow through the reactor was set at 50 cm$^3$ min$^{-1}$ and the gas hourly space velocity (GHSV) was maintained at 15,000 h$^{-1}$. Feed stream to the reactor was prepared by delivering liquid TCE with a syringe pump into dry air, which was metered by a mass flow controller. The injection point was electrially heated to ensure complete evaporation of the TCE. The concentration of TCE in the reaction feeds was set at 1000 ppm. The temperature of the reactor was measured with a thermocouple located just at the bottom of the microreactor.

The effluent gases were analyzed on-line by using two gas chromatographs (GC), one equipped with an electron capture detector (ECD) for the quantitative analysis of the organic chlorinated reactant and products, and the other equipped with a thermal conductivity detector (TCD) for the quantitative determination of CO and $CO_2$. Analysis of both $Cl_2$ and HCl was performed by bubbling the effluent stream through a 0.0125 N NaOH aqueous solution. Then, $Cl_2$ concentration was determined by the titration with ferrous ammonium sulphate (FAS) using *N,N*-diethyl-*p*-phenylenediamine (DPD) as an indicator. The concentration of chloride ions in the bubbled solution was determined by using a chloride ion selective electrode. Furthermore, GC/MS analysis allowed us to confirm the formation of possible by-products or intermediates, such as phosgene ($COCl_2$), tetrachloroethylene (PCE), chloroacetylene ($C_2HCl$) and 1,2-dichloroacetylene ($C_2Cl_2$).

## 3. Results and discussion

### 3.1. Catalyst characterization

Wide angle XRD patterns of the samples obtained at different calcination temperature from the precursor Ce(N-$O_3$)$_3$·6$H_2O$ salt are shown in Fig. 1. It can observed that irrespective of calcination temperature, the XRD patterns of all samples are very similar, showing diffraction peaks at $2\theta = 28.6$, 33.3, 47.5 and 56.4 °, which are characteristic of the cubic fluorite-structured $CeO_2$ [41]. The figure confirms that variations in calcination temperature did not yield any other phases apart from cubic fluorite-structured $CeO_2$. However, the
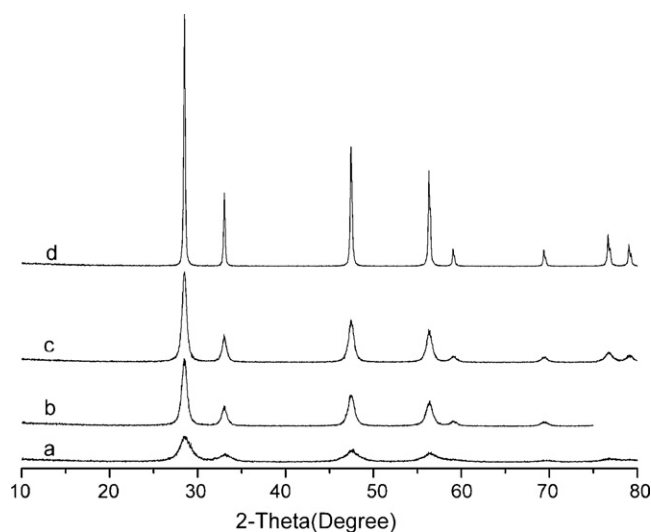
Fig. 1. Wide angel XRD patterns of $CeO_2$ catalysts calcined at different temperature: (a) 450 °C; (b) 550 °C; (c) 650 °C; (d) 800 °C.



Fig. 2. $CO_2$-TPD of $CeO_2$ catalysts calcined at different temperature: (a) 450 °C; (b) 550 °C; (c) 650 °C; (d) 800 °C.

XRD patterns of catalysts revealed differences in the crystalline nature, evident in the differences between peak widths and in the level of background scattering. Crystallite sizes of $CeO_2$ calcined at different temperature based on the diffraction peak broadening are summarized in Table 1. The smallest crystallite size corresponds to the sample calcined at 550 °C (12.1 nm), whereas other samples present crystallite sizes ranging from 12.9 to 36.1 nm. Table 1 also shows other characteristics of the $CeO_2$ samples calcined at different temperature. The surface areas range from 6.5 to 54.6 $m^2\,g^{-1}$. The samples calcined at higher temperature present lower surface areas, 6.5 and 27.9 $m^2\,g^{-1}$, for the samples calcined at 650 and 800 °C, respectively, than those calcined at lower temperature, 53.1 and 54.6 $m^2\,g^{-1}$ for the samples calcined at 450 and 550 °C.

The strength distribution and number of basic sites present in $CeO_2$ samples were investigated by $CO_2$-TPD (shown in Fig. 2). It can be seen that two peaks of $CO_2$ desorption appear over all the $CeO_2$ samples, one at 150–170 °C, corresponding to the weak basic sites, another with the maximum at 325 °C, associated with medium-strength basicity. The basic strength can be controlled by modifying the number of defects in the framework of the materials, i.e. the number of oxygen atoms associated with Ce exhibiting a low coordination number. The sample calcined at 550 °C has a lager amount of defect sites, leading to sites of higher basicity. Raising the calcination temperature to 650 °C or higher, the crystal size of $CeO_2$ grows,
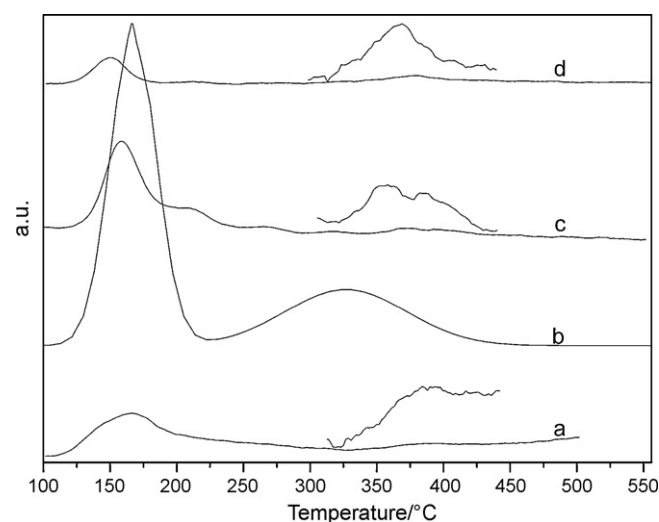
the number of defects will decrease. As a result, the number of oxygen atoms associated with Ce exhibiting low coordination number decreases, and the basicity with medium-strength almost disappears. At the same time, the low-strength basicity is reduced due to the decrease of surface area of the $CeO_2$ samples calcined at higher temperature, such as 800 °C. Additionally, the $CeO_2$ calcined at 450 °C is more stoichiometric (less oxygen vacancies defects) and shows less basicity sites. So, the basicity of $CeO_2$ can be affected largely by the calcination temperature.

In general, oxygen-supplying ability of catalyst depends on the number of oxygen-supplying sites and their activity, which affect catalytic activity of catalysts, especially for total oxidation reactions. So, the mobility of oxygen species in the structure of $CeO_2$ is assessed via $O_2$-TPD. According to Yao's work [43], there existed three types of oxygen in $CeO_2$, i.e. capping, bulk and shared oxygen. Capping oxygen was the most active one, attributed to its mobility, i.e. it could easily exchange with either the oxygen molecules in the gas phase or oxygen species adsorbed on $CeO_2$, which underwent a redox cycle between two oxidation states. Capping oxygen may be produced by the defects in $CeO_2$ crystal whose amount could increase with the thermal impact [40–42]. The other two types of oxygen are more stable and do not have any catalytic activity below 500 °C. In this study, for all $CeO_2$ samples, the $O_2$-TPD appears one strong peak at about 150–190 °C (see Fig. 3). This

Table 1
BET surface area and crystalline sizes of $CeO_2$ catalysts calcined at different temperature

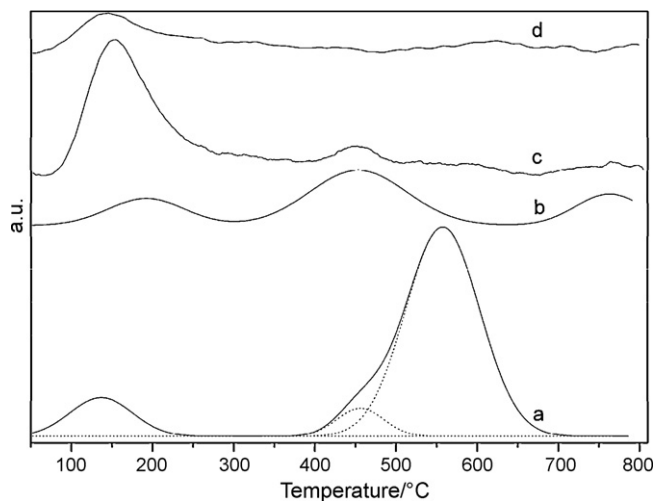| Calcination temperature (°C) | Surface area ($m^2\,g^{-1}$) | Crystalline size (nm) | TPR $H_2$ consumption ($\mu mol\,g^{-1}$) | | | |
|---|---|---|---|---|---|---|
| | | | LT peak | HT peak | | |
| | | | | 400 °C | 550 °C | Total |
| 450 | 53.1 | 12.9 | 28 | 226 | 190 | 419 |
| 550 | 54.6 | 12.1 | 29 | 149 | 241 | 390 |
| 650 | 27.9 | 16.5 | 35 | 137 | 238 | 375 |
| 800 | 6.5 | 36.1 | 20 | 0 | 208 | 208 |

Fig. 3. $O_2$-TPD of $CeO_2$ catalysts calcined at different temperature: (a) 450 °C; (b) 550 °C; (c) 650 °C; (d) 800 °C.

peak is attributed to the physically adsorbed $O_2$ or surface molecular adsorption oxygen species ($O_2^-$) [44–46]. Additionally, the samples calcined at 450, 550 and 650 °C show another peak with the maximum at about 450 °C, which may be attributed to atom oxygen species ($O^-$) [44–46], namely capping oxygen. Moreover, it can be found that the amount of $O_2$ desorption from the sample calcined at 550 °C is larger than those from the samples calcined at 450 and 650 °C. Exceptionally, we find that the sample calcined at 450 °C appears a larger desorption peak at about 550 °C, which likely comes from the desorption of surface lattice oxygen. On increasing the calcination temperature, this oxygen specie can be deviated from $CeO_2$ crystal structure, which results in the formation of non-stoichiometric $CeO_{2-x}$ crystal structure with an amount of defects.

Fig. 4 shows the $H_2$-TPR results of the $CeO_2$ catalysts calcined at different temperature. TPR for the $CeO_2$ catalysts shows two reduction bands between 200 and 750 °C except the
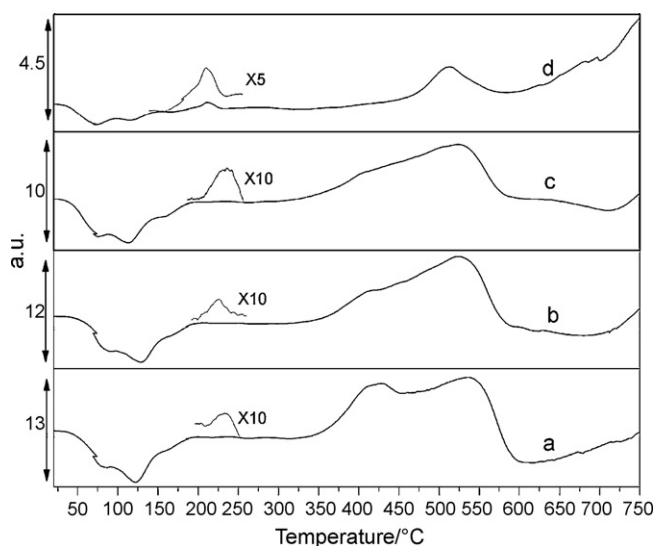


Fig. 4. $H_2$-TPR of $CeO_2$ catalysts calcined at different temperature: (a) 450 °C; (b) 550 °C; (c) 650 °C; (d) 800 °C.

two desorption peaks of $H_2$ or $O_2$ at lower than 150 °C, a small low temperature reduction peak centered at about 210–230 °C (LT peak) and a wide reduction band at higher temperature, from 300 to 600 °C (HT peak) with two maxima centered at ca. 400 (except the $CeO_2$ sample calcined at 800 °C) and 550 °C, respectively. LT peak is related to highly reducible surface ceria species, whereas HT peaks can be attributed to surface reduction of capping oxygen [43]. It must be noted that the reduction of the bulk of $CeO_2$ does not take place in the interval of temperature studied, since it only occurs above 750 °C. Table 1 shows the hydrogen consumption corresponding to LT and HT peaks. It can be see from Table 1, that the hydrogen consumption for the HT peak ranges from 208 to 419 $\mu mol\ g^{-1}$, and the maximal hydrogen consumption value (for $CeO_2$ calcined at 450 °C) is ca. 14% of the theoretical hydrogen consumption (2905 $\mu mol\ g^{-1}$) that would take place for total reduction of $CeO_2$ ($2CeO_2 + H_2 = Ce_2O_3 + H_2O$). Additionally, the hydrogen consumption at 400 °C decreases from 226 to 0 $\mu mol\ g^{-1}$ with the increase of the calcination temperature from 450 to 800 °C. It is probable that the higher calcination temperature easily results in the formation of non-stoichiometric $CeO_2$ ($CeO_{2-x}$, $2 > x > 1.5$), and the $CeO_2$ samples calcined at higher temperature consume less $H_2$ during $H_2$-TPR process. Therefore, the surface lattice oxygen decreases with increase of the calcination temperature, which is consistent with the results of $O_2$-TPD.

XPS spectrum of $CeO_2$ sample calcined at 550 °C is obtained, and the results are shown in Fig. 5. From the spectrum of $Ce_{3d}$, it is observed that there are two sets of spin-orbit multiplets corresponding to $3d_{3/2}$ and $3d_{5/2}$ contributions. $Ce_{3d}$ spectrum contains three main $3d_{5/2}$ features at ca. 881.4, 887.4, and 897.3 eV and three main $3d_{3/2}$ features at ca. 899.6, 906.2, and 915.4 eV. Fujimori [47] has attributed the peaks at 897.3 and 915.4 eV to the transition from the initial state $4f^0$ into the final state $4f^0$. The peaks at 881.4 and 899.6 eV corresponds to the transition from $4f^1$ initial state to $4f^1$ final state and the peaks at 887.4 and 915.4 eV, to $4f^2$ final states arising from ligand-to-4f shake-up transitions from $4f^1$ initial state. The six peaks can be identified in $Ce_{3d}$ spectrum from completely oxidized $CeO_2$. The spectrum of $O_{1s}$ has a single peak at 529.1 eV, which is assigned to the lattice oxygen in $CeO_2$. Two shoulder peaks at ca. 531.0 and 532.7 eV are observed, which can be attributed to adsorbed oxygen or/and weekly bonded oxygen species [43], or to surface oxygen by hydroxyl species and/or adsorbed water species presser as contaminants at the surface. For $CeO_2$ catalyst, oxygen species at the high BE side usually is active oxygen species participating in a reaction, and lattice oxygen supplies and compensates active oxygen via the mobility of oxygen under lean oxygen condition.

## 3.2. Activity tests

In order to check whether some reactions under thermal combustion condition could take place, two "Blank tests", with 3 mm crushed quartz glass (40–60 mush) and without catalyst in the reactor, were carried out. As shown in Fig. 6(A), homogeneous thermal reaction could occur only above 425 °C
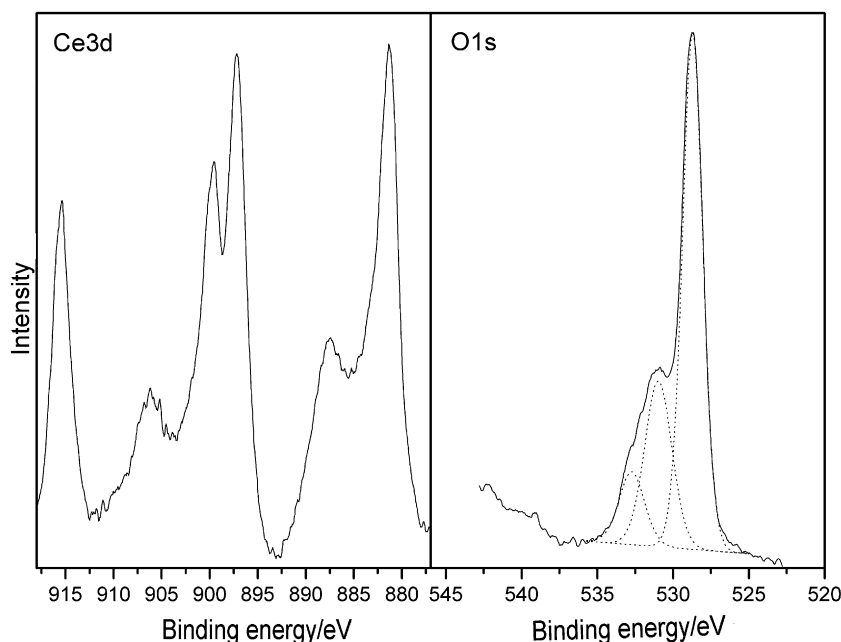
Fig. 5. The $Ce_{3d}$ and $O_{1s}$ spectra of $CeO_2$ catalyst calcined at 550 °C.

to a lower extent. González-Velasco [48] also found homogeneous reaction of TCE with oxygen occurring above 425 °C.

The conversion of TCE on $CeO_2$ catalysts calcined at different temperature as the function of reaction temperature is shown in Fig. 6(B). It can be seen that $CeO_2$ catalysts exhibit high activity for TCE catalytic combustion. And $CeO_2$ calcined at 550 °C appears to be superior for TCE catalytic combustion, and its complete combustion temperature ($T_{90\%}$) of TCE is only 205 °C, which is much lower than those of all catalysts reported in previous literatures, including chromium-based catalysts [16,17]. The activities of $CeO_2$ calcined at 650 and 800 °C are lower than that of $CeO_2$ calcined at 550 °C, which is related to a decrease in BET surface area and an increase in crystallite size (see Table 1). And the lower activity of the sample calcined at 450 °C may be due to the smaller amount of basic sites and active oxygen species.

Based on these results, the best $CeO_2$ catalyst, which is calcined at 550 °C, is used for the following tests unless stated otherwise.

### 3.3. Effect of variable space velocity on TCE catalytic combustion

Fig. 7 shows that the conversion of TCE over $CeO_2$ catalyst as the function of space velocity (GHSV). The conversion over $CeO_2$ catalyst decreases with the increase of space velocity because the residence time for feed molecule through catalyst bed decreases with the increase in space velocity, and a suitably high temperature is needed to achieve a sufficient conversion at a higher space velocity. Additionally, at the space velocity of 15,000 $h^{-1}$, $C_2HCl$ ($m/z = 60$ and 62) and other reaction intermediates are not detected by MS. However, the formation of $C_2HCl$ has been observed at high space velocity (more than 30,000 $h^{-1}$) and the amount of $C_2HCl$ increases with increase of GHSV, that is to say, the selectivity of $C_2HCl$ increases with increase in the space velocity. Furthermore, from the variable space velocity experiments it is also evident that $C_2HCl$ is a reaction intermediate for TCE catalytic combustion over $CeO_2$
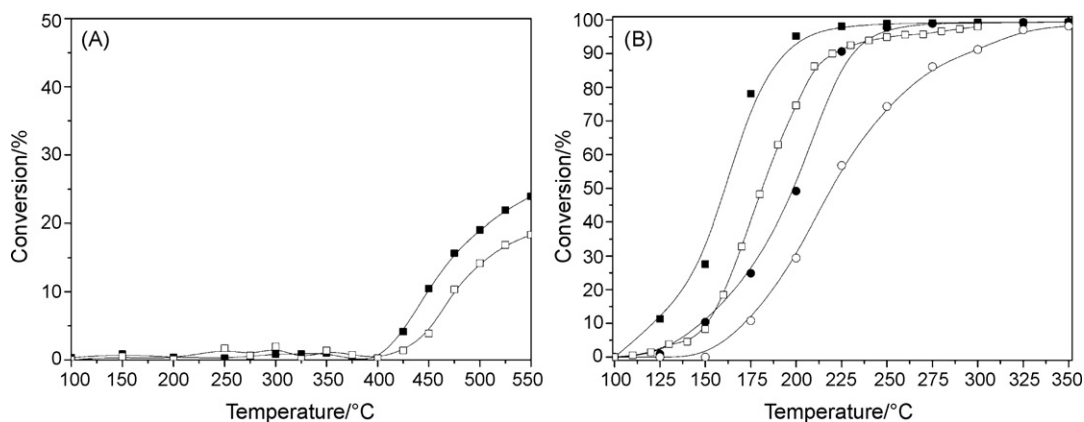


Fig. 6. TCE combustion light-off curves. Gas composition: 1000 ppm TCE, air balance; GHSV = 15,000 $h^{-1}$; (A) blank test: (■) quartz; (□), none; (B) catalytic combustion over $CeO_2$ catalysts calcined at different temperature: (■) 550 °C; (□) 450 °C; (●) 650 °C; (○) 800 °C.

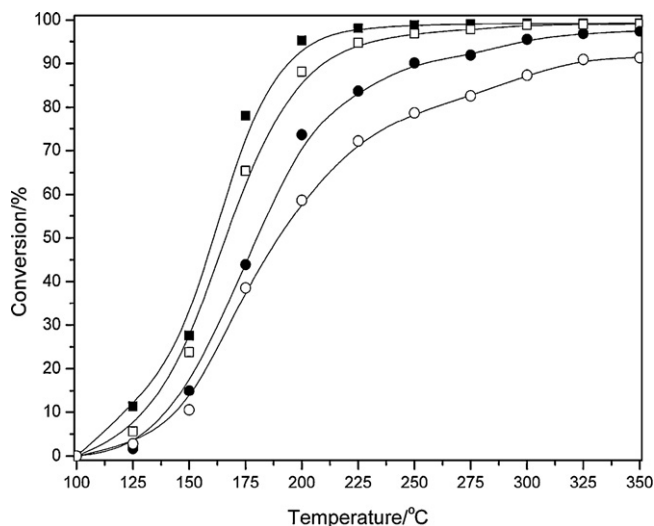Fig. 7. The effect of variable space velocity on TCE catalytic combustion. Gas composition: 1000 ppm TCE, air balance: GHSV: (■) 15,000 h$^{-1}$; (□) 20,000 h$^{-1}$; (●) 30,000 h$^{-1}$; (○) 45,000 h$^{-1}$.

catalyst. Thus, at lower space velocities there is sufficient residence time for $C_2HCl$ molecule to undergo further dissociation and decomposition to $HCl/Cl_2$ and $CO_2/CO$ on active sites (such as basic sites and active oxygen sites) of $CeO_2$ catalysts.

### 3.4. Effect of inlet TCE concentration on TCE catalytic combustion

The effect of the inlet TCE concentration on the conversion of TCE over $CeO_2$ catalyst at the space velocity of 15,000 h$^{-1}$ was investigated. Fig. 8 shows the conversion curves for catalytic combustion of TCE with different concentrations. It can be seen that the conversion of TCE changes mildly with the increase of the inlet TCE concentration from 500 to 1500 ppm, and $CeO_2$ catalyst still shows higher efficiency for catalytic

combustion of low concentration TCE. Therefore, $CeO_2$ catalysts may be used for eliminating higher or lower concentration TCE waste gases. However, at a given temperature, it can be found that the TCE conversion increases appreciably with the increase of TCE inlet concentration. Corella and Padilla [49] also reported the same results.

### 3.5. Effect of water concentration in feed on TCE catalytic combustion

Due to the coexistence of TCE and $H_2O$ in industry waste gases, the effect of water concentration in the feed on the conversion of TCE (1000 ppm) over $CeO_2$ catalyst at the space velocity of 15,000 h$^{-1}$ was investigated and the results are shown in Fig. 9. The destruction efficiency of TCE are decreased by the addition of water, and the presence of water inhibits evidently the catalytic activity of $CeO_2$ catalyst. The inhibition of water probably reflects the competition of water with the TCE molecule for adsorption on the active sites of $CeO_2$ catalyst or water blocks active oxygen sites of the catalyst [50,51]. Interestingly, with the increase of water concentration from 3 to 12% (v/v), TCE conversion increases, and the inhibition of water is found to weaken evidently. Gonzále-Velasco et al. [48] has suggested that the oxidation presented a major pathway for TCE destruction in dry air and in air containing low water contents, whereas hydrolysis was a favored pathway in the presence of excess water. Therefore, the increase of TCE conversion in the feed containing 12% water over $CeO_2$ catalyst probably results from the hydrolysis of TCE.

### 3.6. Effect of water in feed on product distribution

In the case of CVOCs catalytic combustion, the desired reaction is their total oxidation to $CO_2$, $H_2O$ and HCl without other chlorinated by-products and molecular $Cl_2$. The selectivity for HCl and $Cl_2$ over $CeO_2$ catalysts under dry
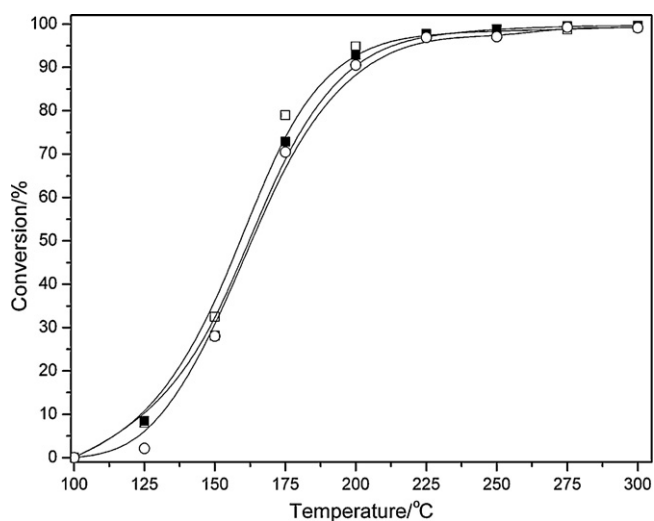


Fig. 8. The light-off curves for TCE catalytic combustion of various inlet TCE concentrations: (○) 500 ppm; (■) 1000 ppm; (□) 1500 ppm; GHSV = 15,000 h$^{-1}$.
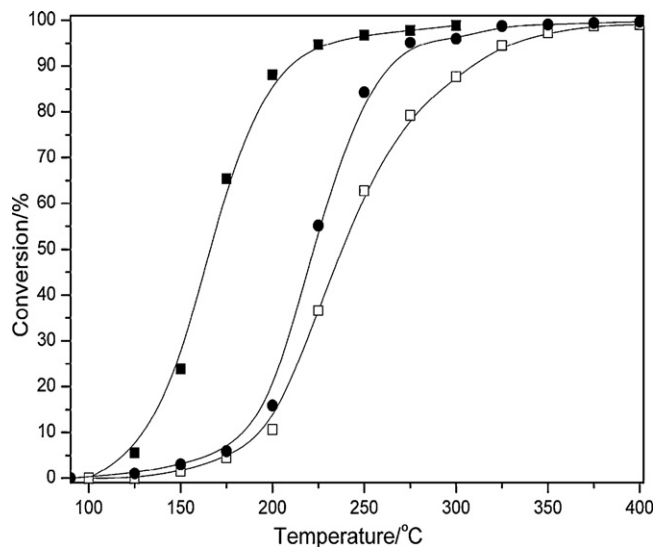


Fig. 9. The light-off curves for TCE catalytic combustion of various water concentrations (v/v): (■) 0%; (□) 3%; (●) 12%; gas composition: 1000 ppm TCE, air balance; GHSV = 15,000 h$^{-1}$.
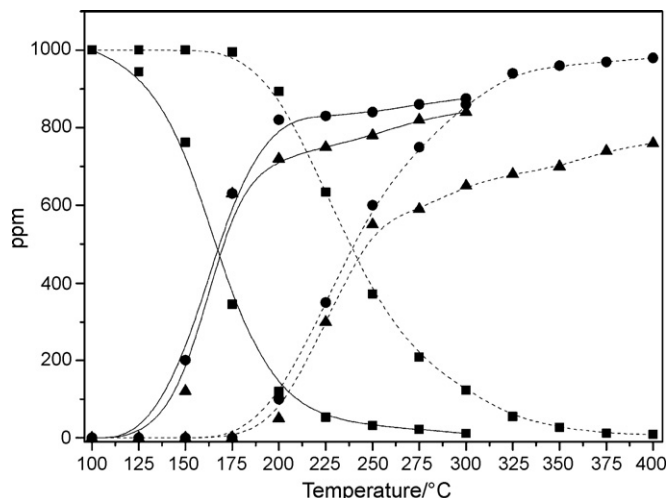
Fig. 10. The selectivity for HCl and Cl$_2$ under dry conditions (–) and humid conditions (- -): (■) TCE; (●) HCl; (▲) Cl$_2$.

and humid conditions (3% water) is shown in Fig. 10. From the concentration curves of HCl and Cl$_2$ as a function of temperature, it can be found that the selectivity for HCl is improved significantly by feeding water and the production of molecular chlorine is greatly lowered at more than 275 °C. That is probably due to that water is dissociated on the surface of CeO$_2$ pre-covered by oxygen into H$^+$ and OH$^-$ species when it is present in the feed, and then the protons recombine with chloride ions interacted with the CeO$_2$ to form HCl, which desorbs from the catalyst surface. Thus, water improves the selectivity for HCl and inhibits the formation of Cl$_2$ to some extent [48]. On the other hand, for the Deacon equilibrium (2HCl + 1/2O$_2$ ⇌ Cl$_2$ + H$_2$O) during catalytic destruction of CVOCs, the thermodynamic equilibrium shifts towards HCl formation in the presence of water. However, whether under dry or humid condition, the chlorine balances are lower than 85% during TCE catalytic destruction over CeO$_2$ catalysts. Poor chlorine balances can be explained by some interactions of CeO$_2$ with HCl or the adsorption of Cl ion on the catalyst surface. In addition, in order to confirm the possible chlorinated organic compounds producing during TCE catalytic combus-

tion, TCE, COCl$_2$, C$_2$Cl$_4$, C$_2$Cl$_2$ and C$_2$HCl are detected by GC/MS in the selective-ion monitoring mode. The results show that no any other chlorinated organic compounds are found except for unreacted TCE.

### 3.7. Catalyst deactivation

For catalytic combustion of CVOCs, the catalyst deactivation is still an involved problem and the industry applications of catalysts are restricted due to poor stability of catalysts. Therefore, in this study, the stability of CeO$_2$ catalysts and their deactivation were investigated, and the results of stability tests are shown in Fig. 11. The catalytic activity of CeO$_2$ catalyst decreases obviously with the reaction run times. After the ninth reaction run, the $T_{50\%}$ value increases from 165 °C up to 325 °C. Additionally, Fig. 11 (b) also shows the plots of the conversion of TCE at 200 °C and 350 °C versus the reaction time under dry and humid conditions. Whether under dry or humid condition, the conversion of TCE drops rapidly after about 10 h of operation at 350 °C. Moreover, it also is found that the catalyst deactivation is more pronounced at lower temperature (200 °C), the activity of the catalyst cannot be maintained for 0.5 h and the conversion drops sharply to 20% within 5 h.

In order to understand the deactivation of CeO$_2$ catalysts, the fresh and the deactivated CeO$_2$ catalysts were characterized and analyzed by TG, EDS, XRD, XPS and Raman. As well known, coking is one of main causes of catalyst deactivation for CVOCs or VOCs catalytic combustion, but EDS and TG results indicate there is no coke deposition on the deactivated CeO$_2$ catalyst (see Fig. 12). XRD results show that there are no CeCl$_3$ and CeOCl phases appearing in bulk as well as on the surface of the deactivated CeO$_2$ catalyst. However, XRD technology is insensitive for the analysis of trace CeCl$_3$ and CeOCl phases. The Raman spectrum shown in Fig. 13 indicates that, the bands at 177, 208 cm$^{-1}$ (CeCl$_3$), and 119, 327 cm$^{-1}$ (CeOCl) are not observed [52]. Combined with the XRD and Raman results, it can be affirmed that CeO$_2$ is not chlorinated to CeOCl and CeCl$_3$ by the chlorine species produced during catalytic combustion of TCE. Thus, the deactivation of CeO$_2$ catalyst
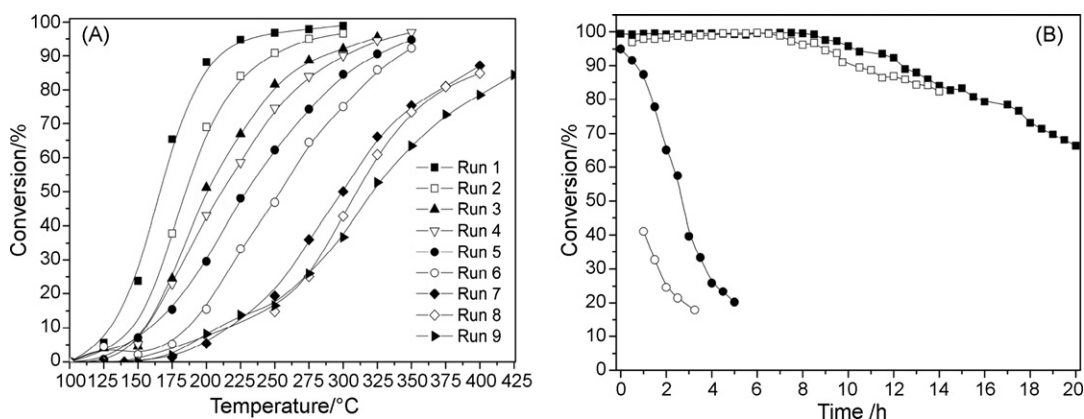


Fig. 11. The stability of CeO$_2$ for TCE catalytic combustion: (A) the reaction runs under dry condition; (B) the reaction under different conditions at constant temperature: (■) 350 °C in dry condition; (□) 350 °C in humid condition; (●) 200 °C in dry condition; (○) 200 °C in humid condition; gas composition: 1000 ppm TCE, air balance; GHSV = 15,000 h$^{-1}$.
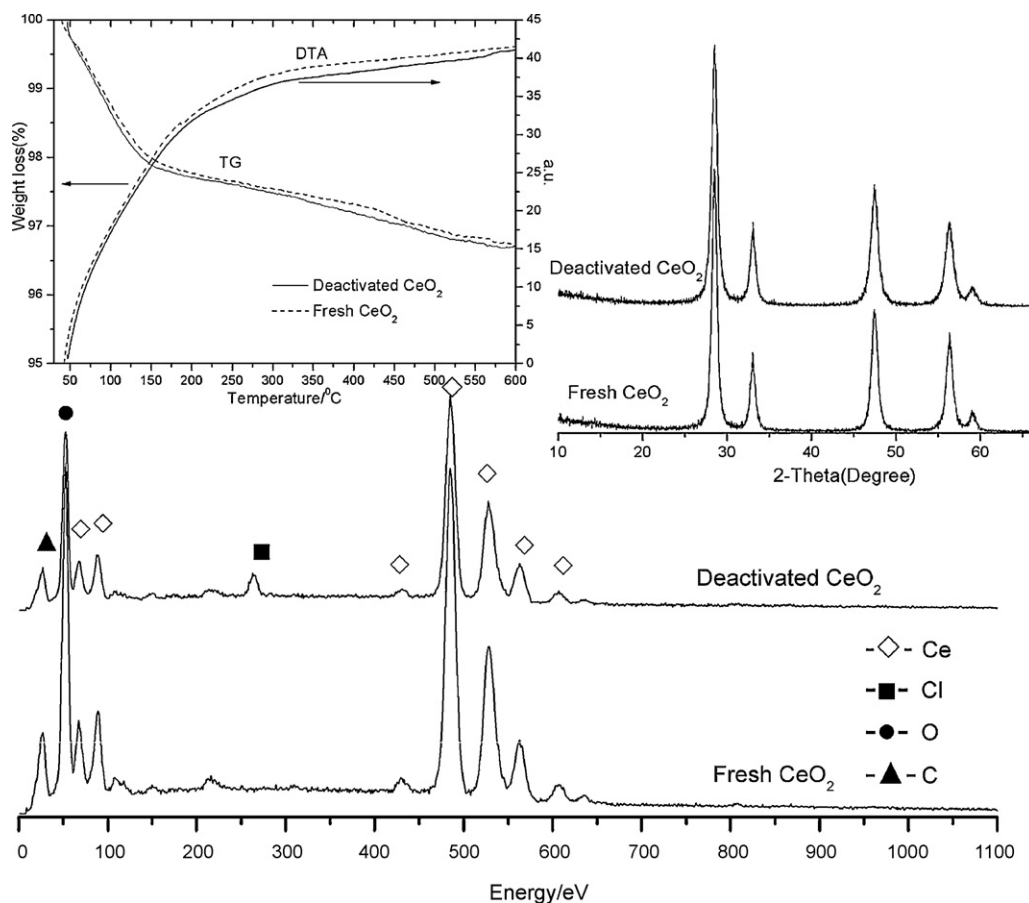
Fig. 12. EDS, TG/DTA and XRD of the fresh and the deactivated $CeO_2$ catalysts.

does not result from the coke deposition on catalyst surface and the formation of non-active species such as CeOCl and $CeCl_3$.

$Cl_{2p}$ peak appearing at around 198 eV on XPS spectrum and the large abundance of Cl element on EDS spectrum, however, confirm the presence of chlorine species on the deactivated $CeO_2$ catalyst. By the comparison of $Ce_{3d}$ peaks of the fresh

$CeO_2$ with those of the deactivated $CeO_2$, it is found that the peaks of the used $CeO_2$ shift 0.4 eV to higher binding energy (see Fig. 14). The strongly electro-negative chlorine species (such as HCl and $Cl_2$) adsorbed on $CeO_2$ catalyst surface make the transition of charge density from cerium atom to Cl atom, and result in shift of binding energy. Therefore, it can be
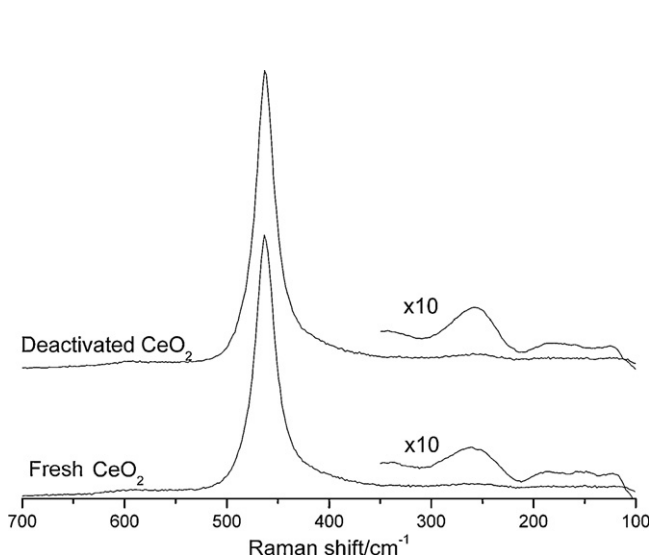


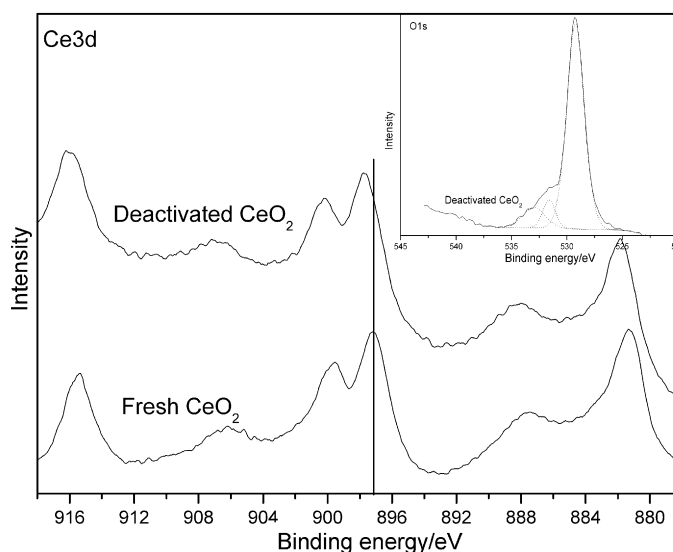Fig. 13. Raman spectra of the fresh and the deactivated $CeO_2$ catalysts.



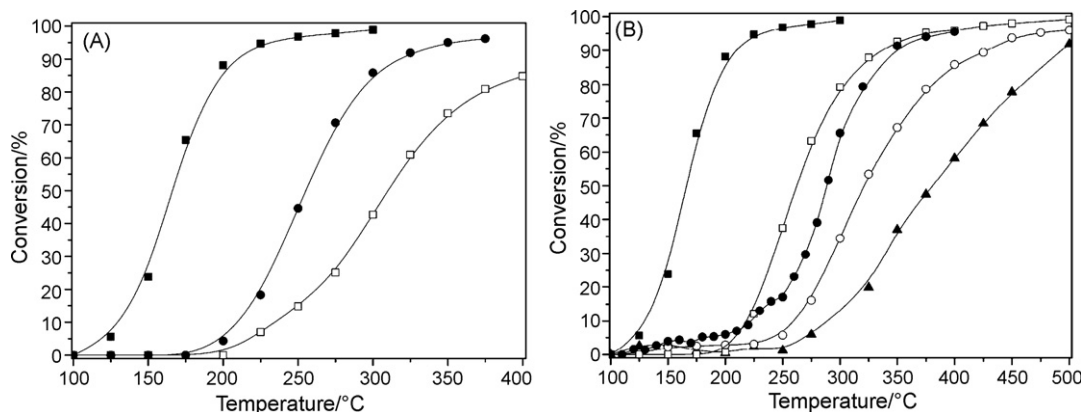Fig. 14. XPS spectra of the fresh and the deactivated $CeO_2$ catalysts.

Fig. 15. The light-off curves for TCE catalytic combustion over $CeO_2$ treated by different treatment methods: (A) (■) fresh $CeO_2$; (●) regenerated $CeO_2$; (□) deactivated $CeO_2$; (B) (■) fresh $CeO_2$; (□) $CeO_2$–HCl–$H_2O$; (●) $CeO_2$–NaCl; (○) $CeO_2$–HCl–Air; (▲) $CeO_2$–HCl.

concluded that the catalyst deactivation is probably due to that HCl or $Cl_2$ strongly adsorbs on the surface of catalyst and blocks the active sites for TCE catalytic combustion. Similar conclusions were drawn by Bond [53] and Windawi [54] who studied the oxidation of CEs over Pt impregnated catalysts.

Compared with $O_{1s}$ spectrum of the fresh $CeO_2$ (Fig. 5), it is observed that, for the deactivated $CeO_2$, the intensities of two shoulder peaks on the high BE side (ca. 531.0 and 532.7 eV) decreases evidently, which indicates that the amount of surface oxygen species ($O_2^-_{(ad)}$ and/or $O^-_{(ad)}$) on $CeO_2$ catalyst are consumed during TCE catalytic combustion. This reveals that the surface oxygen species cannot be compensated rapidly by gas phase oxygen, due to the adsorption and block of chlorine species on the catalyst surface. It may be concluded that surface oxygen species play a key role for TCE catalytic combustion. Therefore, a plausible reaction mechanism of TCE catalytic combustion over $CeO_2$ catalysts is following: TCE associatively adsorbs on the active sites of $CeO_2$ surface and chemisorption takes place by breaking two C–Cl bond. Then a chloroacetylene ($C_2HCl$) intermediate is formed on the $CeO_2$ surface. This intermediate is very reactive and flammable, and can be easily dissociated further by $CeO_2$. The dissociated $C_2HCl$ can be totally oxidized by adsorption oxygen species ($O^-$), and form $CO_2$, CO and $H_2O$.

The adsorption behavior of HCl or $Cl_2$ was investigated by assistant experiments. The deactivated $CeO_2$ was treated by sweeping with humid airflow (12% (v/v) of water) at 550 °C for 4 h. Fig. 15 (A) shows light-off curve of the regenerated $CeO_2$ catalyst. The catalytic activity of the deactivated $CeO_2$ is recovered evidently by the sweeping of humid airflow, and the $T_{50\%}$ value decreases from 310 to 250 °C. Noticeably, in another test as shown in Fig. 11(B), the presence of water does not improve the stability of $CeO_2$ catalyst. It is deduced that the removal or displace of chlorine species adsorbed on active sites is very difficult and slow, even water is present in the reaction system.

In order to confirm further that $CeO_2$ catalyst deactivation results from the strong adsorption of Cl ion on catalyst surface, $CeO_2$ was treated by HCl to get chloride ion-containing $CeO_2$ samples and the activity was measured under the space velocity

of 15,000 $h^{-1}$ with the feed of 1000 ppm TCE under dry condition. Fig. 15(B) shows the conversion of TCE over $CeO_2$–HCl decreases sharply comparing with the fresh $CeO_2$, and the temperature of 50% conversion increases from 165 to 380 °C. Therefore, the strong adsorption of Cl ion on active sites must result in the deactivation of $CeO_2$, which is confirmed by XPS, because the $Ce_{3d}$ and $O_{1s}$ spectrum of $CeO_2$–HCl are same with that of fresh $CeO_2$. However, HCl as a strong acid possibly has effect on surface properties of $CeO_2$ catalyst such as surface basicity, and the basicity of $CeO_2$ catalyst is important for the catalytic combustion of TCE. In order to eliminate the effects of acid, $CeO_2$ was treated by the neutral NaCl salt aqueous solution. The catalytic activity of $CeO_2$–NaCl also decreases sharply (see Fig. 15(B)). Therefore, it can be affirmed that $CeO_2$ catalyst deactivation results from the strong adsorption of Cl ion on the catalyst surface. Additionally, the TCE conversion of $CeO_2$–HCl or $CeO_2$–NaCl increases obviously after swept in dry air or humid air at 550 °C for 4 h, and the effect of humid air is better than dry air. The determination of Cl ion on the regenerated $CeO_2$ surface by EDS confirmed that the strong adsorption of Cl ion on the catalyst surface may be removed by sweeping of humid air, but the removal of chlorine or chloride from the surface is a slow step. It can be inferred that, if the sweeping time is enough long, the activity of the treated $CeO_2$ may be recovered completely.

Therefore, to improve the stability of the $CeO_2$ catalyst, it is necessary to remove or transfer rapidly the chlorine or chloride adsorbed on the catalyst surface so as to exposure the active sites for TCE catalytic combustion.

## 4. Conclusion

Catalytic combustion of TCE over $CeO_2$ catalysts was experimentally studied. $CeO_2$ catalysts exhibit high activity for TCE catalytic combustion. The better catalytic behavior of $CeO_2$ catalysts is attributed to surface basicity, high mobility of oxygen and oxygen-supplying ability of $CeO_2$ catalysts.

The formation of $C_2HCl$ as a reaction intermediate is observed at higher than 30,000 $h^{-1}$ space velocity, and TCE of lower than 500 ppm concentration can be decomposed

effectively. Main products of TCE catalytic combustion over $CeO_2$ catalysts are HCl, $Cl_2$, $CO_2$ and a trace of CO, and other by-products such as tetrachloroethylene are not detected.

The presence of water in the feed influences the catalytic destruction of TCE over $CeO_2$ catalysts. TCE destruction is inhibited evidently at lower water concentration (3%), but enhanced to a certain extent at higher water concentration (12%), which suggests that TCE destruction occurs via both hydrolysis and oxidation under humid condition. Additionally, HCl selectivity is much improved with the addition of water to the feed by the combination of hydrogen species with chlorine attached to the catalyst surface.

$CeO_2$ catalysts are very active for TCE catalytic combustion, but their activity quickly diminishes due to the strong adsorption of HCl or $Cl_2$ produced from the decomposition of TCE and the block of active sites (such as basic sites and active oxygen sites) of $CeO_2$. Cl adsorbed strongly on catalyst surface may be removed by sweeping of humid air, but the removal of chlorine or chloride ions from $CeO_2$ surface is a slow step.

## Acknowledgment

## References

[1] W.K. Jo, K.H. Park, Chemosphere 57 (2004) 555.
[2] M. Mohseni, A. David, Appl. Catal. B 46 (2003) 219.
[3] B. Immaraporn, P.P. Ye, A.J. Gellman, J. Catal. 223 (2004) 98.
[4] Y.C. Amorim, P.M. Patterson, M.A. Keane, J. Catal. 234 (2005) 68.
[5] O.W. Nishijim, T.Y. Tsai, Y. Nakano, M. Okada, Appl. Catal. B 51 (2004) 135.
[6] J.D. Ortego, J.I. Richardson, M.V. Twigg, Appl. Catal. B 12 (1997) 339.
[7] J.N. Coute, J.D. Ortego, J.T. Richardson, M.V. Twigg, Appl. Catal. B 19 (1998) 175.
[8] T.E. McMinn, F. Craig Moates, J.T. Richardson, Appl. Catal. B 31 (2001) 93.
[9] M. Magureanu, N.B. Mandache, J. Hu, R. Richards, M. Florea, V.I. Parvulescu, Appl. Catal. B 76 (2007) 275.
[10] M. Guillemot, J. Mijoin, S. Mignard, P. Magnoux, Appl. Catal. B 75 (2007) 249.
[11] A. Musialik-Piotrowska, Catal. Today 119 (2007) 301.
[12] B. Mendyka, A. Musialik-Piotrowska, K. Syczewska, Catal. Today 11 (1992) 597.
[13] R.S. Krishnamoorthy, J.A. Rivas, M.D. Amiridis, J. Catal. 193 (2000) 264.
[14] S.K. Agarwal, J.J. Spivey, J. B. Butt. Appl. Catal. A 82 (1992) 259.
[15] R. Rachapudi, P.S. Chintawar, H.L. Greene, J. Catal. 185 (1999) 58.
[16] S. Chatterjee, H.L. Greene, Y.J. Park, J. Catal. 138 (1992) 179.
[17] K.-E. Jeong, D.-C. Kim, S.-K. Ihm, Catal. Today 87 (2003) 29.
[18] F. Bertinchamps, M. Treinen, P. Eloy, A.-M. Dos Santos, M.M. Mestdagh, E.M. Gaigneaux, Appl. Catal. B 70 (2007) 360.
[19] F. Bertinchamps, C. Grégoire, E.M. Gaigneaux, Appl. Catal. B 66 (2006) 1.
[20] J.I. Gutie'rrez-Ortiz, B. de Rivas, R. Lo'pez-Fonseca, S. Martín, J.R. González-Velasco, Chemosphere 68 (2007) 1004.
[21] S. Imamura, Catal. Today 11 (1992) 547.
[22] M.E. Swanson, H.L. Greene, S. Qutubuddin, Appl. Catal. B 52 (2004) 91.
[23] R. Lopez-Fonseca, A. Aranzabal, J.I. Gutierrez-Ortiz, J.I. Alvarez-Uriarte, J.R. Gonzalez-Velasco, Appl. Catal. B 30 (2001) 303.
[24] R. Lopez-Fonseca, B. de Rivas, J.I. Gutierrez-Ortiz, A.A. Aranzabal, J.R. Gonzalez-Velasco, Appl. Catal. B 41 (2003) 31.
[25] R. Lopez-Fonseca, J.I. Gutiérrez-Ortiz, M.A. Gutierrez-Ortiz, J.R. Gonzalez-Velasco, J. Catal. 209 (2002) 145.
[26] R. Lopez-Fonseca, J.I. Gutiérrez-Ortiz, J.L. Ayastui, M.A. Gutierrez-Ortiz, J.R. Gonzalez-Velasco, Appl. Catal. B 45 (2003) 13.
[27] R. Lopez-Fonseca, J.I. Gutiérrez-Ortiz, J.R. Gonzalez-Velasco, Catal. Commun. 5 (2004) 391.
[28] M. Taralunga, J. Mijoin, P. Magnoux, Catal. Commun. 7 (2006) 115.
[29] M. Guillemot, J. Mijoin, S. Mignard, P. Magnoux, Appl. Catal. A 327 (2007) 211.
[30] P. Zimmer, A. Tschöpe, R. Birringer, J. Catal. 205 (2002) 339.
[31] B. Skårman, D. Grandjean, R.E. Benfield, A. Hinz, A. Andersson, L.R. Wallenberg, J. Catal. 211 (2002) 119.
[32] Y. Liu, T. Hayakawa, K. Suzuki, S. Hamakawa, T. Tsunoda, T. Ishii, M. Kumagai, Appl. Catal. A 223 (2002) 137.
[33] X.L. Tang, Y. Li, Y.D. Xu, Q. Xin, W.J. Shen, Catal. Today 93-95 (2004) 191.
[34] T.X.T. Sayle, S.C. Parker, D.C. Sayle, Phys. Chem. Chem. Phys. 7 (2005) 2936.
[35] W. Liu, M. Flytzanistephanopoulos, J. Catal. 153 (1995) 304.
[36] P. Knauth, G. Schwitzgebel, A. Tschöpe, S. Villain, J. Solid State Chem. 140 (1998) 295.
[37] S. Imamura, I. Fukuda, S. Ishida, Ind. Eng. Chem. Res. 27 (1988) 718.
[38] V.S. Mishra, V.V. Mahajani, J.B. Joshi, Ind. Eng. Chem. Res. 34 (1995) 2.
[39] B. de Rivas, R. López-Fonseca, J.R. González-Velasco, J.I. Gutíerrez-Ortiz, J. Mol. Catal. A 278 (2007) 181.
[40] S.S. Lin, C.L. Chen, D.J. Chang, C.C. Chen, Water Res. 36 (2002) 3009.
[41] S.S. Lin, D.J. Chang, C.H. Wang, C.C. Chen, Water Res. 37 (2003) 793.
[42] C.H. Wang, S.S. Lin, Appl. Catal. A 268 (2004) 227.
[43] H.C. Yao, Y.F. Yu Yao, J. Catal. 86 (1984) 254.
[44] L. Xue, C.B. Zhang, H. He, Y. Teraoka, Appl. Catal. B 75 (2007) 167.
[45] H. He, H.X. Dai, C.T. Au, Catal. Today 90 (2004) 245.
[46] A. Bielański, J. Haber, Catal. Rev. Sci. Eng. 19 (1979) 1.
[47] A. Fujimori, Phys. Rev. B 27 (1983) 3392.
[48] J.R. González-Velasco, A. Aranzabal, R. López-Fonseca, R. Ferret, J.A. González-Marcos, Appl. Catal. B 24 (2000) 33.
[49] T.J. Corella, J.M. Toledo, A.M. Padilla, Appl. Catal. B 27 (2000) 243.
[50] R. Lopez-Fonseca, S. Cibrián, J.I. Gutiérrez-Ortiz, J.R. González-Velasco, Stud. Surf. Sci. Catal. 142 (2002) 841.
[51] M. Kulazyński, J.G. van Ommen, J. Trawczyński, J. Walendziewski, Appl. Catal. B 36 (2002) 239.
[52] D.Y. Hase, M.L.A. Temperini, Spectrochim. Acta 8 (1981) 597.
[53] G.C. Bond, N. Sadeghi, J. Appl. Chem. Biotechnol. 25 (1975) 241.
[54] H. Windawi, M. Wyatt, Platinum Met. Rev. 37 (1993) 186.